

Numerical Modeling and Performance Prediction of COS Hydrolysis Reactor in Integrated Gasification Fuel Cell in terms of Thermo-Chemical Transport Phenomena

Jung-Hun Noh¹, Dong-Shin Ko¹, Sung-Jong Lee², Deog-Jae Hur^{1*}

¹R&D Center for Research & Business Cooperation Mechatronics Team, Institute for
Advanced Engineering, Korea

*Corresponding author. Tel.: +82-31-330-7418; fax: +82-31-330-7116.

E-mail address: djhur@iae.re.kr (D.-J. Hur)

Abstract

During the recent decades, global warming by greenhouse gas evolution has attracted worldwide attention and evermore strict regulations thereon have become institutionalized as international policies. In the process, more environment-friendly power generation technologies have been developed utilizing fossil fuels with a view to timely commercialization. As one of such “clean coal” technology, Integrated Gasification Fuel Cell system is a promising power generation means and COS hydrolysis reactor is installed downstream of coal syngas to remove acidic gas constituents such as H_2S and COS. The most significant design parameters affecting performance of the COS hydrolysis reactor were selected to be GHSV, (catalytic) reaction temperature, and length ratio and numerical modeling was performed considering heat and fluid flow transfer as well as chemical reaction kinetics. Effect of the selected design parameters on the variation of conversion rate and reactant gas mixture concentration were comprehensively investigated to predict performance of COS hydrolysis reactor. Stochastic modeling of reactor performance was finally performed using Monte Carlo simulation and linear regression fitting.

Keywords: COS hydrolysis Reactor, numerical analysis, thermo-chemical transport phenomena, Monte Carlo simulation

Nomenclature

C_p	specific heat, J/kg-K
C_k	mass fraction of each species
$C_{1\varepsilon}$	constant
$C_{2\varepsilon}$	constant
$C_{3\varepsilon}$	constant
D_{bed}	diameter of reactor, m
D_{cat}	diameter of catalyst, m
D_k	diffusivity of each species, m ² /s
E	activation energy, kJ/mol
G_b	production of turbulence kinetic energy due to buoyancy, kg/s ³ -m
G_k	production of turbulence kinetic energy due to the mean velocity gradient,
kg/s ³ -m	
H_{bed}	length of reactor, m
k	turbulence kinetic energy, m ² /s ²
k_{eff}	effective conductivity, W/m-K
k_1	constant
K_3	constant
M	molar weight, g/mol
P	pressure, Pa
P_{COS}	partial pressure of COS, Pa
P_{H_2O}	partial pressure of H ₂ O, Pa
r_{COS}	reaction rate of COS, mol/h-g

S_e	heat source, W/m ³
S_k	source term of each species, kg/m ³ -s
t	time, s
T	temperature, K
\vec{u}	velocity, m/s
V_{inlet}	velocity of inlet, m/s
ε	dissipation rate of turbulent kinetic energy, m ² /s ³
θ	sphericity
μ	viscosity, Pa-s
μ_t	turbulent viscosity, Pa-s
v	group contribution value
ρ	density, kg/m ³
σ_k	turbulent Prandtl number for k
σ_ε	turbulent Prandtl number for ε
ϕ	porosity

1. Introduction

Recent worldwide concerns on global warming and environmental pollution have been at their zenith and Integrated Gasification Combined Cycle and similar “clean coal technology” for energy supply have attracted renewed technological interests for power generation. In the similar context, Integrated Gasification Fuel Cell technology of Fig. 1 has been introduced as nearly “zero emission clean coal technology” and related R & D has been conducted in full swing [1]. Syngas produced by coal gasification contains various acidic gases (H_2S , COS), particulates, minute quantities of HCl, NH_3 and heavy metal elements. These inherently undesirable constituents should be properly removed for subsequent operation of fuel cell installed downstream. A series of apparatuses are used to remove acidic gases and COS hydrolysis reactor is presently selected for numerical modeling to estimate its performance in terms of operational and geometrical parameters.

Literature on COS hydrolysis research had been concentrated on kinetics of catalyst or reaction mechanism thereof. Fiedorow et al. performed extensive study on kinetics and relevant mechanistic experiment using alumina catalyst and its COS hydrolysis performance [1-5]. On the other hand, Bachelier et al. investigated into catalytic activity of various oxide catalysts [6]. Guo also performed COS hydrolysis study especially related to its advancement on catalytically active area of alkali metal oxides at 45~100 °C [7]. Wang et al. studied on how to improve catalytic activity of Al_2O_3 under low humidity condition as well as adsorption study to remove COS [8]. Similar adsorption of COS on activated carbon was also investigated by Shunzheng et al. [9-10] and they also performed on COS removal efficiency using metallic catalyst and activated carbon [11-14]. COS hydrolysis study using noble metal catalysts was also performed by Zhang and Yang who evaluated catalytic removal efficiency of such noble metal catalysts [15-16].

In the present study, COS hydrolysis reactor as an acidic gas removal unit of Integrated Gasification Fuel Cell system is numerically modeled to evaluate various design parameters. Chemical reaction kinetics were also modeled in the process as well as heat and fluid transfer phenomena. Using the numerical analysis modeling thus developed, prediction formula was derived to stochastically evaluate and analyze effects of various operational and geometrical parameters on COS hydrolysis reactor

performance. Finally, guidance criteria on optimized operation of COS hydrolysis reactor was suggested based on such numerical modeling analysis results.

2. Numerical Model Development

2.1 COS hydrolysis reactor model

Performance analysis of the COS hydrolysis reactor was evaluated via numerical modeling with variation of operational and geometrical parameters. Such modeling result was used to derive relevant parameters affecting reactor performance for proper guidance criteria on efficient reactor design.

Schematic diagram of COS hydrolysis reactor used in the present study is shown in Fig. 2. Gaseous reactant mixture containing COS is introduced to upper tube. The reactant gas is transported to the lower part of the reactor, entering into the catalyst layer of Kaiser 201. Heat is supplied to the reactor via external heater to activate catalytic reaction. A portion of reactant gas mixture is converted into products after passing through the catalyst layer and the reacted gas mixture exits via lower exhaust pipe. COS hydrolysis reaction is generally affected by gas temperature, sensitive to operational parameter such as GHSV, and it also depended on reactor geometry.

For quantitative analysis of transport properties within the COS hydrolysis reactor, internal heat and fluid transfer behavior of gas had to be numerically modeled as well as ensuing chemical reactions. For heat and fluid behavior modeling, commercially available ANSYS Fluent 18.0 software was used: user-defined function mode enabled numerical modeling of specific chemical reactions. The relevant governing equations for heat and fluid behavior modeling and chemical reaction analysis are described by Eq (1) ~ (6).

➤ Mass conservation equation

$$\frac{\partial \rho}{\partial t} + \nabla \cdot (\rho \vec{u}) = 0 \quad (1)$$

➤ Momentum conservation equation

$$\frac{\partial(\rho \vec{u})}{\partial t} + \nabla \cdot (\rho \vec{u} \vec{u}) = -\nabla p + \nabla \cdot (\mu \nabla \vec{u}) \quad (2)$$

➤ Transport equation for κ (standard k- ϵ model)

$$\frac{\partial(\rho k)}{\partial t} + \nabla \cdot (\rho k \vec{u}) = \nabla \cdot \left[\left(\mu + \frac{\mu_t}{\sigma_k} \right) \nabla k \right] + G_k + G_b - \rho \epsilon \quad (3)$$

➤ Transport equation for ϵ (standard k- ϵ model)

$$\frac{\partial(\rho \epsilon)}{\partial t} + \nabla \cdot (\rho \epsilon \vec{u}) = \nabla \cdot \left[\left(\mu + \frac{\mu_t}{\sigma_\epsilon} \right) \nabla \epsilon \right] + C_{1\epsilon} \frac{\epsilon}{k} (G_k + G_{3\epsilon} G_b) + C_{2\epsilon} \rho \frac{\epsilon^2}{k} \quad (4)$$

➤ Energy conservation equation

$$\frac{\partial(\rho C_p T)}{\partial t} + \nabla \cdot (\rho C_p T \vec{u}) = \nabla \cdot (k_{eff} \nabla T) + S_e \quad (5)$$

➤ Species transport equation

$$\frac{\partial(C_k)}{\partial t} + \nabla \cdot (C_k \vec{u}) = \nabla \cdot (D_k \nabla C_k) + S_k \quad (6)$$

Internal fluid flow analysis within the COS reactor was made using mass and momentum conservation equations while turbulent flow was numerically modeled by standard k- ϵ model for turbulence analysis. On the other hand, species transport equation was solved to analyze pertinent chemical reactions, numerically analyzing formation and depletion of reactant gas species and quantitatively giving their concentrations. Reaction kinetics under prevailing parameter condition was modeled using empirically-derived kinetics and user-defined function enabled calculation and integration at real time basis. Lastly, energy equation was used to incorporate heat transfer as affected by internal heater and heat energy variation as affected by chemical reaction.

2.2 Kinetics and mathematical model of catalyst bed

Kaiser 201 catalyst was used to activated COS hydrolysis reaction and its properties are listed in detail in Table 1. The catalyst was of spherical morphology and available in constant diameter of 5 mm. Its main constituent is Al_2O_3 and high catalyzing area enabled improved reaction efficiency.

Numerical analysis of COS hydrolysis reactor necessitated mathematical modeling of the catalyst layer. Porous medium morphology concept was introduced to simulate fluid behavior of the catalyst area. Such porous medium modeling was justified in view of the near-impossible modeling for the individual layer of packed catalysts and cost-effectiveness, assuming completely spherical and consistent geometry of catalyst layer to incorporate resistance to fluid flow. Such modeling concept is schematically depicted in Fig. 3 and pertinent Ergun equation is written as Eq. (7) to account for pressure drop caused by fluid resistance.

➤ Ergun Equation (Porous Medium)

$$\frac{dP}{dL} = \frac{150\mu(1-\phi)^2}{\theta^2 D_{cat}^2 \phi^3} \bar{u} + \frac{1.75\rho(1-\phi)}{\theta D_{cat} \phi^3} \bar{u}^2 \quad (7)$$

Viscous and inertia losses are accounted for by the first and second term of Ergun equation as applied to a porous medium. Such fluid resistance was used to numerically model reactant gas mixture flow down the catalyst packed layer.

Reaction advancement of the COS hydrolysis reaction is determined by empirically-derived kinetics. Experimentally substantiated kinetics was thus applied in the present study for numerical modeling of reaction kinetics [17]. COS hydrolysis reaction and relevant kinetics are represented by Eq. (8) and Eqs. (9) ~ (11), respectively.

➤ Kinetics of COS hydrolysis reaction (Kaiser 201)



$$-r_{cos} = k_1 K_3 \frac{P_{cos} P_{H_2O}}{1 + K_3 P_{H_2O}} \quad (9)$$

Here,

$$k_1 = \exp\left(0.835 - \frac{3.039 \times 10^3}{T}\right) \quad (10)$$

$$K_3 = \exp\left(-15.89 + \frac{1.001 \times 10^4}{T}\right) \quad (11)$$

Reaction kinetics was simulated by Eley-Rideal model, where individual modeling parameter was empirically determined. The significant parameters affecting reaction rate were partial pressure of gas reactant mixture and temperature which determined reaction kinetics with utmost sensitivity.

2.3 Properties and boundary conditions of COS hydrolysis reactor

Properties of individual gaseous constituent in the reactant gas mixture is systematically listed in Table 2 for accurate and comprehensive numerical modeling of COS hydrolysis reactor, mainly citing NIST(National Institute of Standard and Technology) data.

Inter-diffusion coefficients of major gaseous constituents were calculated using Eq. (12) from Perry's Chemical Engineer's Handbook [18].

➤ Binary-Diffusivity

$$D_{12} = \frac{0.01013T^{1.75}\left(\frac{1}{M_1} + \frac{1}{M_2}\right)^{0.5}}{P\left[(\sum \nu_1)^{1/3} + (\sum \nu_2)^{1/3}\right]^2} \quad (12)$$

The binary diffusivity equation predicts inter-diffusion coefficients using molecular weight and structure at a specific temperature and pressure and the calculated inter-diffusion coefficients are accurate within $\pm 5\%$.

The present numerical modeling necessitates operational parameters to predict performance of the COS hydrolysis reactor. The present modeling was based on ordinary boundary condition with upper and lower limits suitable for proper evaluation of COS hydrolysis reactor with variation of operational parameters.

Table 3 summarizes pertinent boundary conditions for COS hydrolysis reactor. At first, objective

hourly capacity of 200 Nm³/h was converted to velocity which was varied to estimate its effect on reactor performance. Inlet gas temperature and chemical composition were specified considering overall IGFC process gas temperature and composition: the gas temperature was also carefully cross-checked with variation of internal heater temperature.

2.4 Numerical Procedures

Numerical modeling of the COS hydrolysis reactor was performed via reactor geometry and the boundary condition for ensuing analysis where 2-dimensional axi-symmetry model was used for efficient analysis using commercially available ANSYS Fluent 18.0 heat and fluid analysis software. User-defined function mode of the ANSYS Fluent 18.0 was used to calculate kinetic data which were reflected into the relevant governing equation via source term. The elements for numerical modeling numbered 54,173 ~ 129,814 and the coupled governing equations were obtained by trial and error calculation using finite volume method and SIMPLE algorithm. For actual analysis, convergence condition was taken to be less than 10⁻⁵ of relative uncertainty level

3. Results and discussion

The previously suggested geometry and operational parameters of COS hydrolysis reactor were used to evaluate its performance. In detail, concentration variation of COS and its conversion rate were compared to ascertain individual effect of the modeling parameters. For this, 3 levels of GHSV, length ratio, and temperature were selected for evaluation of operational and geometrical parameter, as listed in Table 4: Length ratio is a geometrical factor of the reactor tube and is defined by Eq. (13).

$$R_{length} = \frac{H_{cat}}{D_{cat}} \quad (13)$$

All in all, effects of reactor tube diameter and its length on overall performance were investigated under similar GHSV condition.

Fig. 4 illustrates heat and fluid flow analysis results for reference modeling (GHSV = 1.0, length ratio = 1.0, Temperature = 573 K). Fig. 4 (a) depicts pressure distribution in the reactor, confirming development of relatively high stagnant pressure at the catalyst area where reactant gas mixture enters into high resistance catalytic layer with high porosity. Fig. 4 (b) shows modeling result of velocity field, showing jet-type velocity distribution via reactant gas mixture entering into the (reactor) tube inlet and then rapidly decreasing its velocity by uniform distribution among the catalytic pores. Fig. 4 (c) shows temperature contour afforded by the external heat supply along the reactor tube wall surface, explaining reactor gas temperature increase. The catalytic layer with high thermal conductivity solid area (porosity 0.4) enabled simultaneous heat convection and transfer, thus confirming high heat transport efficiency.

Fig. 5 schematically shows modeling analysis result on reference model (GHSV = 1.0, length ratio = 1.0, Temperature = 573 K). More specifically, Fig. 5 (a) shows concentration contour of reacting (COS, H₂O) gases, highest concentration at the inlet of the catalytic layer and gradual reduction in concentration with passage into the porous catalytic layer. The reactant flow is concentrated into the central portion of the catalytic layer by inlet tube and renders slow reaction rate caused by low thermal energy from the external heater. Reactant concentration is thus maintained high and such effect became insignificant with passage into the reaction area. On the other hand, H₂S and CO₂ product gas concentration increases with passage into the catalytic reaction area. Reaction rate of the reactants render low concentration at the central region and such effect is gradually annulled with passage into the outlet. Fig. 5 (c) graphically illustrates reactant concentration, products concentration, and temperature variation at the center of the reactor: reactants concentration rapidly decreases as they pass reaction zone, while proportionately increasing products concentration.

Eq. (14) was used to evaluate reactor performance based on the concentration contour of COS gas at the inlet and outlet of the reactor. Catalytic conversion rate of COS is defined as ratio of reacted COS concentration to the originally supplied COS concentration at the inlet of the reactor, COS conversion rate of the reference model being 41.1%.

$$CR_{COS} = \frac{(C_{COS,inlet} - C_{COS,outlet})}{C_{COS,inlet}} \times 100 \quad (14)$$

Temperature variation inside of the reactor showed delayed response caused by the transport of the heat energy supplied by external heater, changing reaction rate and affecting reactor performance.

Conversion rate of the reactant gas mixture was estimated and compared using the suggested numerical modeling to analyze effects of individual parameters. Fig. 6 shows conversion rate, concentration and temperature variation with GHSV. Fig. 6 (a) graphically depicts conversion rate variation with GHSV, showing maximum 50.1% conversion rate with increase in GHSV. This is attributed to increased GHSV for equivalent amount of catalyst, thus decreasing conversion rate. The concentration and temperature variation of Fig. 6 (b) clearly illustrates slow catalytic reaction with GHSV via reduction in temperature by increased reactant gas mixture flow and increased reactant mass renders slower decrease in reactant gas concentration. All in all, low GHSV increases reactor temperature and activates reaction further to result in higher reaction rate. Besides, COS concentration rapidly decreased by relatively small quantity of reactants. GHSV selection is thus very important for optimized reactor design.

Secondly, the effect of length ratio on reactor performance was investigated by variation of diameter and its length. Fig. 7 shows effect of length ratio on conversion rate, concentration and temperature variation. At first, Fig. 7 (a) graphically shows conversion rate and maximum 9.2% was possible with increase in length ratio for the same GHSV and reactor tube wall temperature. Fig. 7 (b) shows effect of length ratio on COS concentration inside of the reactor and temperature: COS concentration rapidly decreased with length ratio while temperature increased proportionally. This is attributed to facile heat transfer and radial gas diffusion in the tube via reduction in reactor diameter and increased tube length, respectively, causing increased reaction rate. Therefore, optimized length ratio could result in higher COS conversion rate.

Lastly, effect of external heater temperature on the reactor wall was investigated by comparing external tube wall temperature. Fig. 8 shows effects of reactor wall temperature on conversion rate,

reactant concentration and inside temperature of the reactor. Fig. 8 (a) shows variation of conversion rate with temperature on the reactor wall (547~603 K), showing maximum 19.3% increase in COS conversion rate for the same GHSV and length ratio. Fig. 8 (b) also shows effects of variation of reactant gas concentration and reactor temperature inside on the reaction rate and conversion rate, mainly confirming beneficial effect of reactor wall temperature. This cogently shows that higher heater temperature is required for high COS conversion rate. However, higher heater temperature ensures more energy consumption and enhanced GHSV is more important than heater temperature increase, thus requiring optimization of other operational variables such as GHSV, length ratio before finalizing reactor wall temperature for more efficient operation of COS hydrolysis reactor.

In view of the previously performed numerical modeling analysis results, regression analysis was made incorporating GHSV, length ratio, temperature, and conversion rate, Eq. (15) ~ (18).

$$CR_{\text{cos}} = 41.1 - 22.3A + 3.1B + 7.0C + 3.1A^2 - 0.8B^2 - 0.4AB \quad (15)$$

Here,

$$A = 1.44 \ln(\text{GHSV}) - 15.83 \quad (16)$$

$$B = 0.96 \ln(R_{\text{length}}) - 0.88 \quad (17)$$

$$C = 0.03T_{\text{wall}} - 19.1 \quad (18)$$

Fig. 9 schematically compares Eq. (15) and numerically modeled COS conversion rate, showing accuracy of $\pm 10\%$. Based on this result, Monte Carlo simulation was made for sensitivity confirmation of individual parameters considering probability distribution characteristics of GHSV, length ratio, and temperature for estimation of COS conversion rate.

Monte Carlo simulation is usually performed by adopting stochastic model for probabilistic distribution of a specific parameter with uncertainty involved. In general, analytical solution is possibly obtained for definitely defined model but stochastic model usually does not guarantee such solution. Numerical modeling is thus needed for analytic solution and probability distribution of a specific

parameter should be obtained by trial and error method.

For that purpose, performance parameters of a COS hydrolysis reactor were chosen to be GHSV, length ratio, and temperature to estimate performance efficiency via probability analysis within variation range of individual parameters. For this, variation ranges of GHSV, length ratio, and temperature were selected to be $10,000 \sim 15,000 \text{ h}^{-1}$, $0.884 \sim 7.062$, and $543 \sim 603 \text{ K}$, respectively. Variation range was taken as 3σ level considering reasonably efficient reactor performance and normal distribution with relevant average and standard deviation values, as listed in Table 4. Table 5 lists distribution of individual performance parameters obtained by using normalization of individual performance parameters as specified in Table 4.

In application of Monte Carlo simulation, more than 1,000,000 random numbers were created for increased probabilistic credibility. Variation of individual performance parameter was defined within 3σ level considering credible level of operational control. Fig. 8 illustrates COS conversion rate for sensitivity of performance parameter and its distribution. Fig. 8 (a) was obtained by limiting variation range of GHSV and temperature within 3σ level and more than 95% of conversion rate efficiency with reliability level of 98.9%. On the other hand, sensitivity of COS performance efficiency was evaluated in Fig. 8 (b) and temperature, GHSV, and length ratio were rated as important to be 57.3 (temperature) and -38.6% (GHSV). Therefore, GHSV and temperature should be controlled within tolerable margin for efficient performance improvement of the COS reactor.

4. Conclusions

In the present study, a numerical modeling approach was used for heat and fluid transfer and conversion reaction prevailing in the COS hydrolysis reactor of an IGFC syngas production plant. Various performance parameters and their individual effect on the reactor performance were investigated with main emphasis placed on method of numerical modeling result analysis. The following analysis results are summarized.

- With other parameters fixed, COS conversion rate decreased with GHSV. This is attributed to increased reactant amount afforded by higher GHSV, thus decreasing conversion rate of COS.
- COS conversion rate increased by 9.2% with length ratio under the same GHSV and reactor tube wall temperature. This is caused by the more facile heat transfer and gas diffusion along and inside of the reactor tube for larger length ratio.
- COS conversion rate increased by maximum 19.3% with reactor wall temperature with the GHSV and length ratio unchanged. However, this ensures higher energy cost and more efficient setting of temperature is needed.
- Monte Carlo simulation was performed under 3σ level for more stable and reliable operation control level and operational process efficiency was modeled within individual parameter variation range. This confirmed maximum possible COS conversion rate of 95% with reliability level of 98.9%.
- Within limit of sensitivity evaluation of individual parameters, temperature was rated as the most sensitive (57.3%) with GHSV as the next most sensitive (-38.6%) parameter.
- Design of experiment method was suggested to estimate numerical modeling analysis method considering COS conversion rate and probability distribution of design and operational parameters for COS hydrolysis reactor design. Monte Carlo simulation was also performed for more efficient stochastic analysis and estimate.

The present numerical modeling and analysis method could ensure more accurate estimate of COS hydrolysis reaction for more efficient design criteria. More specifically, heat and fluid transfer and COS conversion within the (catalytic) reaction area inside of the COS reactor were comprehensively modeled for more reliable estimate of operation and design of COS reactor.

Acknowledgment

This work was supported by the Korea Institute of Energy Technology Evaluation and Planning(KETEP) and the Ministry of Trade, Industry & Energy(MOTIE) of the Republic of Korea (No. 20163010050080).

References

- [1] Fiedorow, R., Leaute, R., and Dalla Lana, I. G. 1984, "A study of the kinetics and mechanism of COS hydrolysis over alumina," *Journal of Catalysis*, Vol. 85, No. 2, pp. 339~348.
- [2] Huang, H., Young, N., Williams, B. P., Taylor, S. H. and Hutchings, G., 2005, "COS hydrolysis using zinc-promoted alumina catalysts," *Catalysis Letters*, Vol. 104, No.1-2, pp. 17~21.
- [3] Huang, H., Young, N., Williams, B. P., Taylor, S. H. and Hutchings, G., 2006, "High temperature COS hydrolysis catalysed by γ -Al₂O₃," *Catalysis letters*, Vol. 110, No.3-4, pp. 243~246.
- [4] Hoggan, P. E., Aboulayt, A., Pieplu, A., Nortier, P. and Lavalley, J. C., 1994, "Mechanism of COS hydrolysis on alumina," *Journal of Catalysis*, Vol. 149, No.2, pp. 300~306.
- [5] John, W., 2001, "Ni-and Zn-promotion of γ -Al₂O₃ for the hydrolysis of COS under mild conditions," *Catalysis Communications*, Vol. 2(3-4), pp. 135~138.
- [6] Bachelier, J., Aboulayt, A., Lavalley, J. C., Legendre, O. and Luck, F., 1993, "Activity of different metal oxides towards COS hydrolysis. Effect of SO₂ and sulfation," *Catalysis today*, Vol. 17, No. 1-2, pp. 55~62.
- [7] Shishao, T., Chunhu, L., Shengzhao, L. and Hanxian, G., 1991, "Compensation effect in catalytic hydrolysis of carbonyl sulfide at lower temperature compensation effect in COS hydrolysis," *Catalysis Letters*, Vol. 8, No.2-4, pp. 155~167.
- [8] Wang, L., Wang, S., Yuan, Q. and Lu, G., 2008, "COS hydrolysis in the presence of oxygen: Experiment and modeling," *Journal of Natural Gas Chemistry*, Vol. 17, No.1, pp. 93~97.
- [9] Wang, X., Ma, Y., Ning, P., Qiu, J., Ren, X., Li, Z., and Liu, W., 2014, "Adsorption of carbonyl sulfide on modified activated carbon under low-oxygen content conditions," *Adsorption*, Vol. 20, No. 4, 623~630.

- [10] Wang, H. Y., Yi, H. H., Tang, X. L., Yu, L. L., He, D. and Zhao, S. Z., 2010, "Effect of Preparation Conditions on Catalytic Hydrolysis of COS," *In: Management and Service Science (MASS), 2010 International Conference on. IEEE*, pp. 1~4.
- [11] Wang, X., Qiu, J., Ning, P., Ren, X., Li, Z., Yin, Z., and Liu, W., 2012, "Adsorption/desorption of low concentration of carbonyl sulfide by impregnated activated carbon under micro-oxygen conditions," *Journal of hazardous materials*, Vol. 229, pp. 128~136.
- [12] Yi, H. H., Wang, H. Y., Tang, X. L., Yu, L. L. and Yang, L. N., 2010, "Effect of Catalyst Composition on catalytic hydrolysis of COS," *In Power and Energy Engineering Conference (APPEEC), 2010 Asia-Pacific IEEE.*, pp. 1~4.
- [13] Ping, N., Lili, Y. U., Honghong, Y. I., Xiaolong, T. A. N. G., Hua, L. I., Hongyan, W. and Lina, Y., 2010, "Effect of Fe/Cu/Ce loading on the coal-based activated carbons for hydrolysis of carbonyl sulfide," *Journal of Rare Earths*, Vol. 28, No.2, pp. 205~210.
- [14] Sun, X., Ning, P., Tang, X., Yi, H., Li, K., He, D. and Lai, R., 2014, "Simultaneous catalytic hydrolysis of carbonyl sulfide and carbon disulfide over Al₂O₃-K/CAC catalyst at low temperature," *Journal of Energy Chemistry*, Vol. 23, No. 2, pp. 221~226.
- [15] Zhang, Y., Xiao, Z. and Ma, J., 2004, "Hydrolysis of carbonyl sulfide over rare earth oxysulfides," *Applied Catalysis B: Environmental*, Vol. 48, No.1, pp. 57~63.
- [16] Yang, Y., Shi, Y. and Cai, N., 2016, "Simultaneous removal of COS and H₂S from hot syngas by rare earth metal-doped SnO₂ sorbents," *Fuel*, Vol. 181, pp. 1020~1026.
- [17] Tong, S., Dalla Lana, I. G. and Chuang, K. T., 1995, "Kinetic modeling of the hydrolysis of carbon disulfide catalyzed by either titania or alumina," *The Canadian Journal of Chemical Engineering*, Vol. 73, No.2, pp. 220~227.
- [18] Green, Don W., and Robert H. Perry., 1973, *Perry's Chemical Engineers' Handbook/edición Don W. Green y Robert H. Perry*. No. C 660.28 P47 2008..

List of tables

Table 1. Material and chemical composition of Kaiser 201 catalyst.

Table 2. Physical properties of working fluid at 473.15K and 1,950 kPa.

Table 3. Case for numerical analysis.

Table 4. Normal distribution of operating and geometrical parameters.

Table 5. Distribution of normalized parameters.

Table 1

Description	Value	Unit
Shape	Sphere	-
Diameter	4.5 ~ 5.0	mm
Surface Area	296	m ² /g
Al₂O₃	93.60	%(by wt.)
SiO₂	0.20	%
Fe₂O₃	0.02	%
TiO₂	0.02	%
Na₂O	0.30	%

Table 2

Description	Density [kg/m ³]	Viscosity [Pa-s]	Specific Heat [J/kg-K]	Thermal Conductivity [W/m-K]
H ₂	0.91	1.22 × 10 ⁻⁵	14,522	0.269
CO	13.79	2.49 × 10 ⁻⁵	1,071	0.038
H ₂ S	17.48	2.06 × 10 ⁻⁵	1,137	0.031
COS	31.40	2.30 × 10 ⁻⁵	850	0.032
N ₂	13.78	2.53 × 10 ⁻⁵	1,063	0.037
H ₂ O	9.80	1.61 × 10 ⁻⁵	3,169	0.042

Table 3

	Condition	Value	Unit
Inlet	Velocity	4.9 ~ 19.6	m/s
	Temperature	473	K
	Mass Fraction	H ₂	0.019
		CO	0.675
		H ₂ S	0.573×10^{-3}
		COS	0.880×10^{-4}
		N ₂	0.156
		H ₂ O	0.031
		CO ₂	0.117
			-
Outlet	Pressure Outlet	-	-
Wall	Constant Temperature	543 ~ 603	K

Table 4

Case	GHSV [h ⁻¹]	Length Ratio [-]	Temperature [K]
1	29,214	0.35	543
2			573
3			603
4		1.00	543
5			573
6			603
7		2.83	543
8			573
9			603
10	58,429	0.35	543
11			573
12			603
13		1.00	543
14			573
15			603
16		2.83	543
17			573
18			603
19	116,858	0.35	543
20			573
21			603
22		1.00	543
23			573
24			603
25		2.83	543
26			573
27			603

Table 5

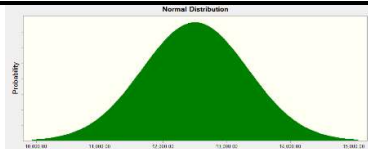
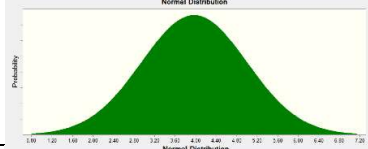
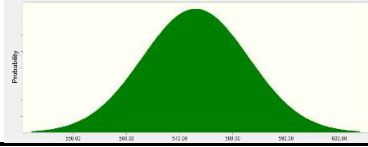
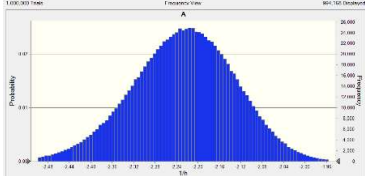

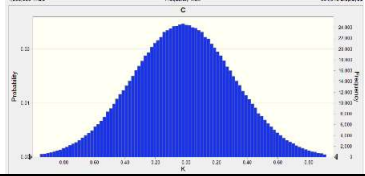
Parameter	Mean Value	Standard Deviation	Distribution
GHSV [h ⁻¹]	12,500	833	
Length Ratio [-]	3.97	1.03	
Temperature [K]	573	10	

Table 6

Normalized Parameter	Mean Value	Standard Deviation	Distribution
A	2.23	0.10	
B	0.39	0.35	
C	0.02	0.33	

List of figure

Figure 1. Schematic diagram of integrated coal gasification fuel cell combined cycle.

Figure 2. Geometric diagram of COS hydrolysis reactor.

Figure 3. The concept of Porous medium for catalyst bed.

Figure 4. Predicted results of COS hydrolysis reactor; (a) pressure, (b) velocity, (c) temperature.

Figure 5. Predicted results of COS hydrolysis reactor; (a) reactant, (b) product, (c) concentration profiles.

Figure 6. Predicted results of COS hydrolysis reactor according to GHSV; (a) COS conversion rate, (b) COS concentration and temperature profiles.

Figure 7. Predicted results of COS hydrolysis reactor according to length ratio; (a) COS conversion rate, (b) COS concentration and temperature profiles.

Figure 8. Predicted results of COS hydrolysis reactor according to temperature; (a) COS conversion rate, (b) COS concentration and temperature profiles.

Figure 9. Comparison of COS conversion rate between proposed regression equation and the numerical data.

Figure 10. Probability distribution of COS conversion rate and Sensitivity of performance parameters in COS hydrolysis reactor.

Figure 1

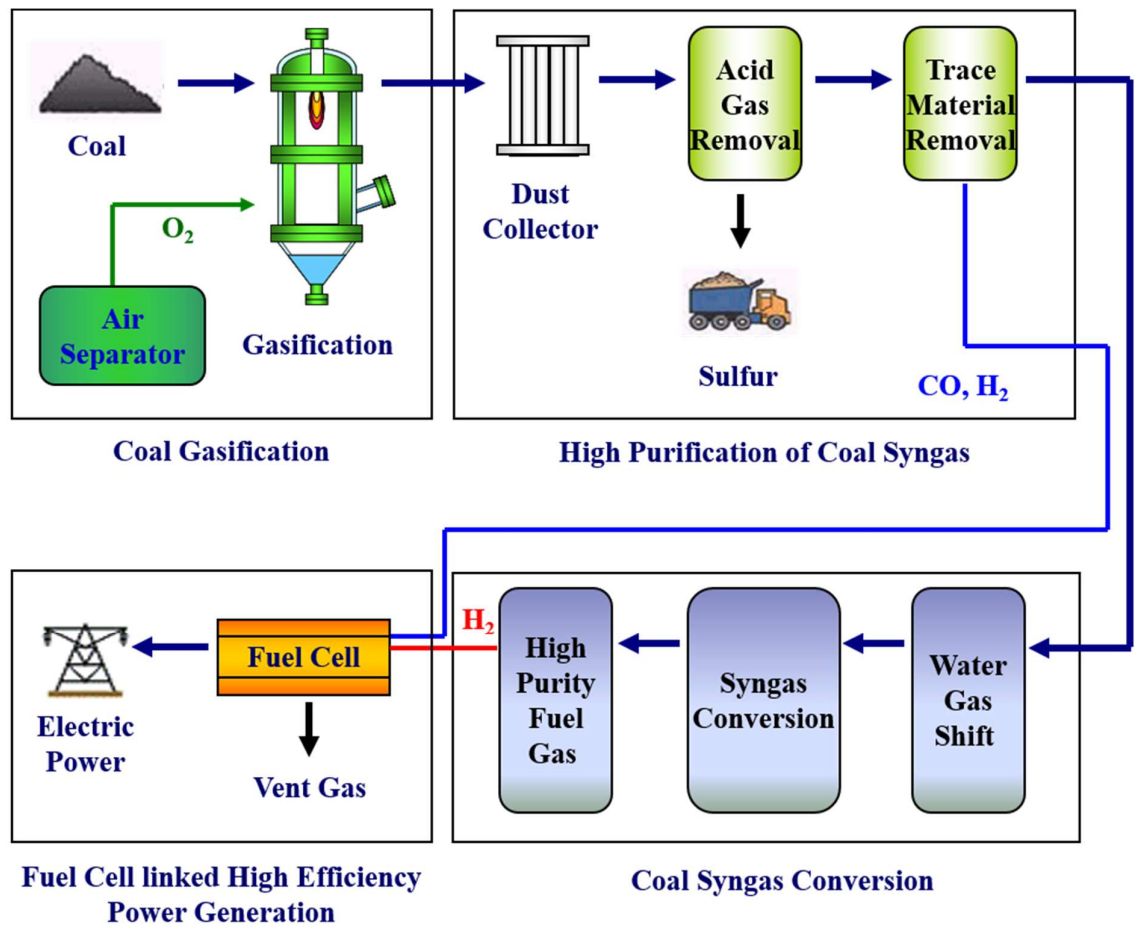


Figure 2

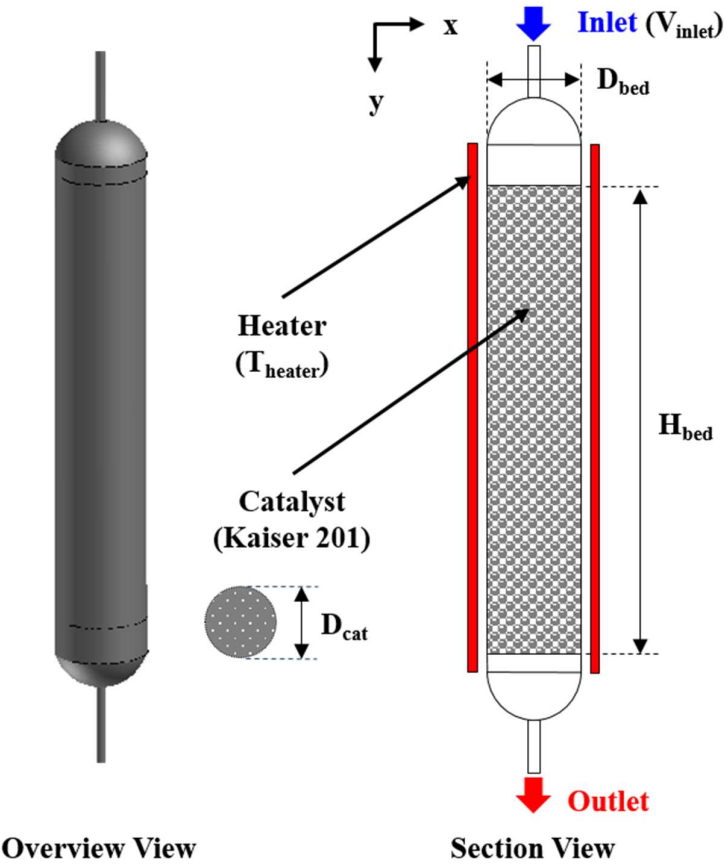


Figure 3

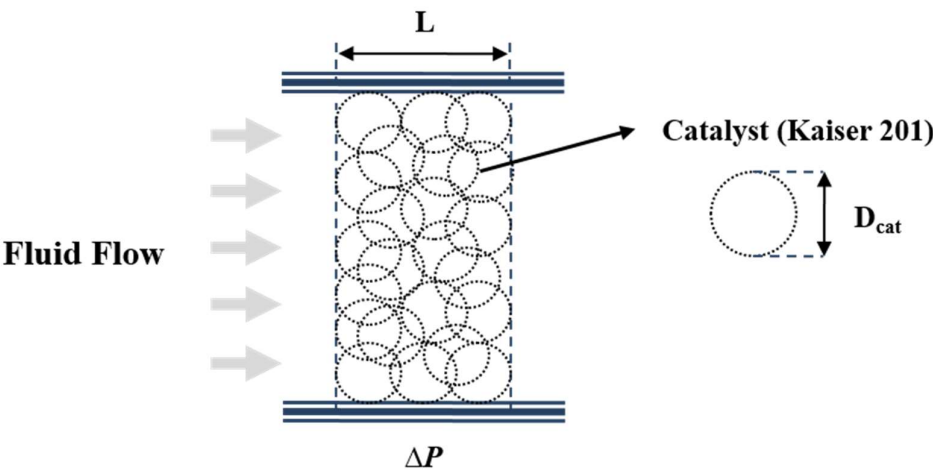


Figure 4

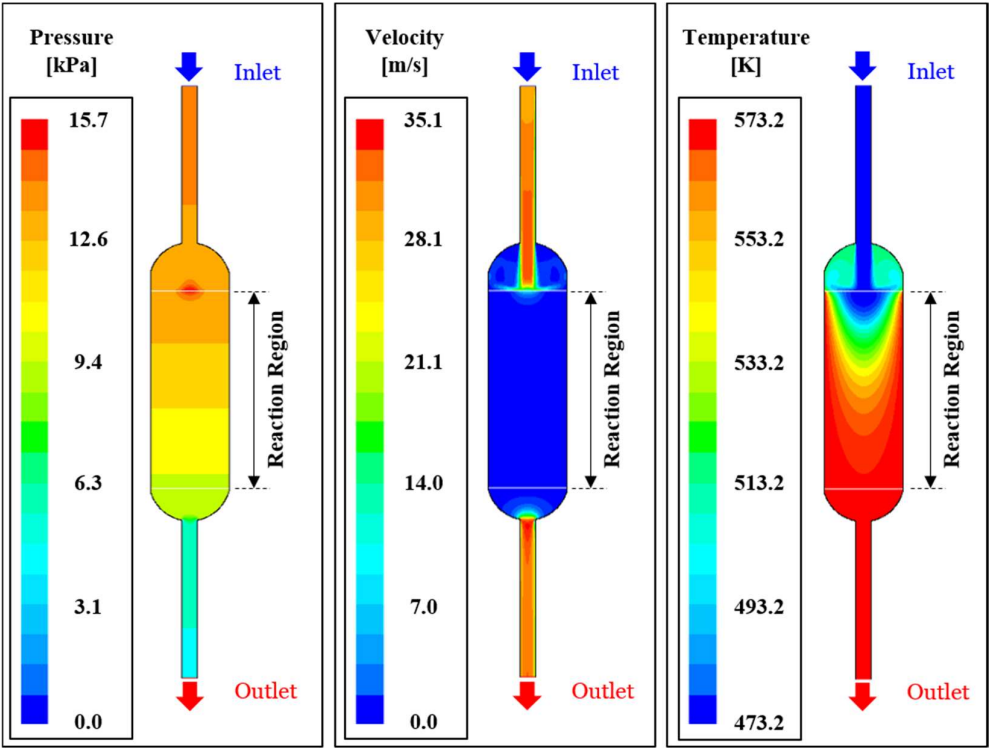
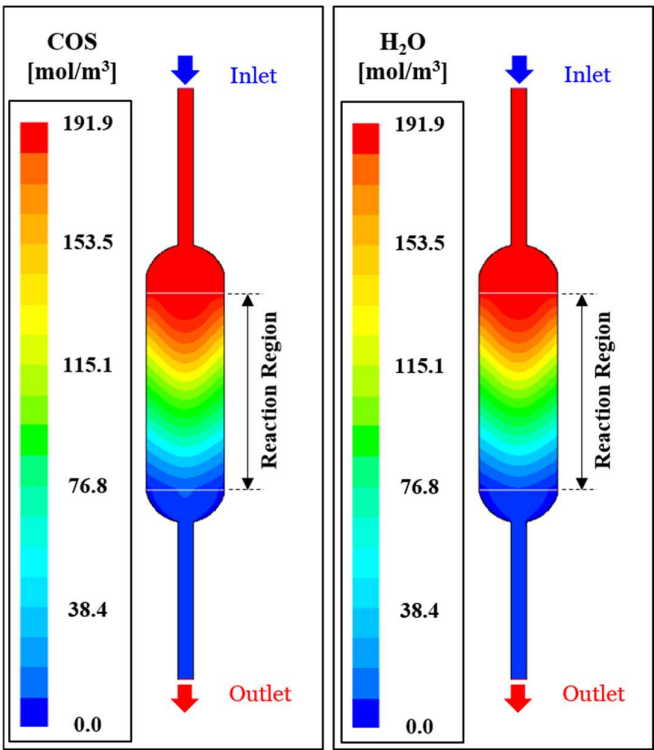
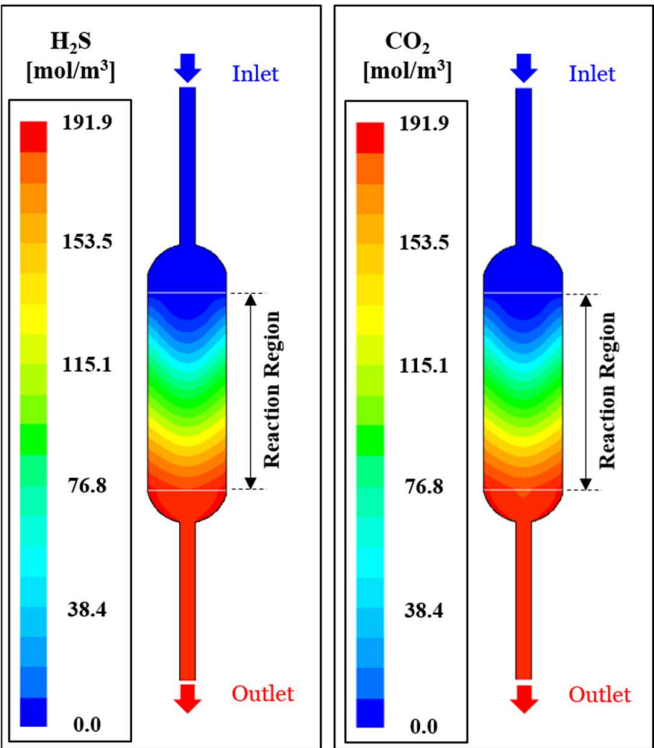


Figure 5

(a)



(b)



(c)

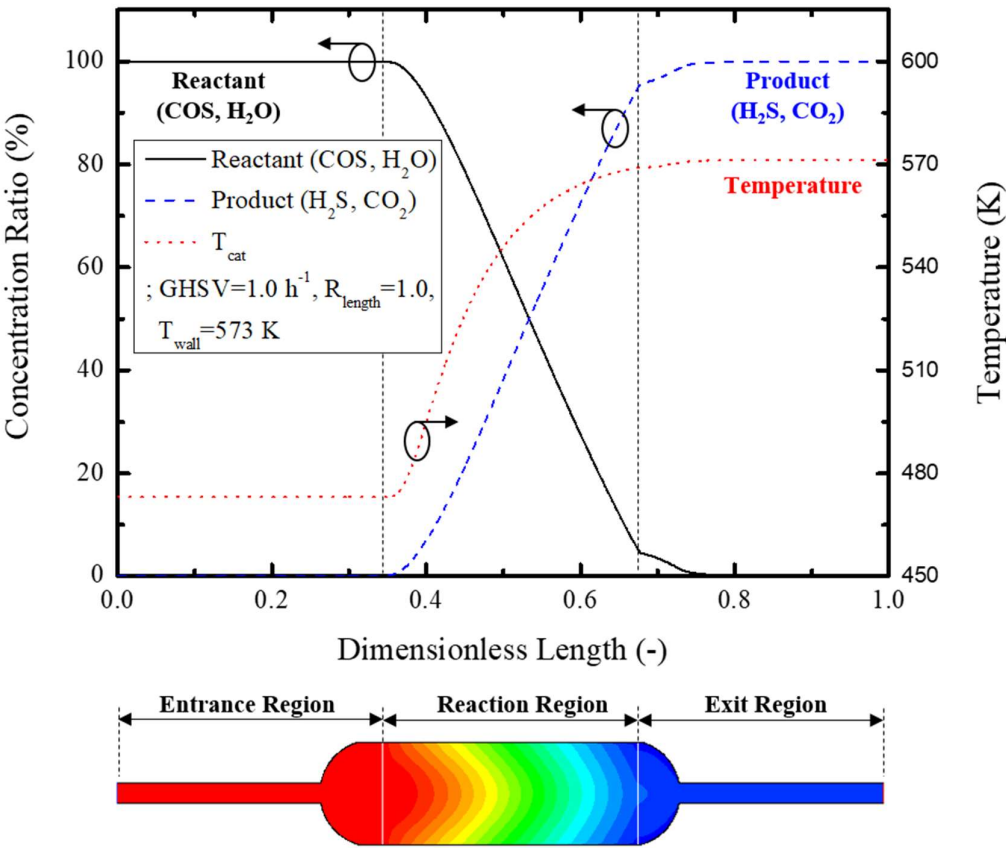
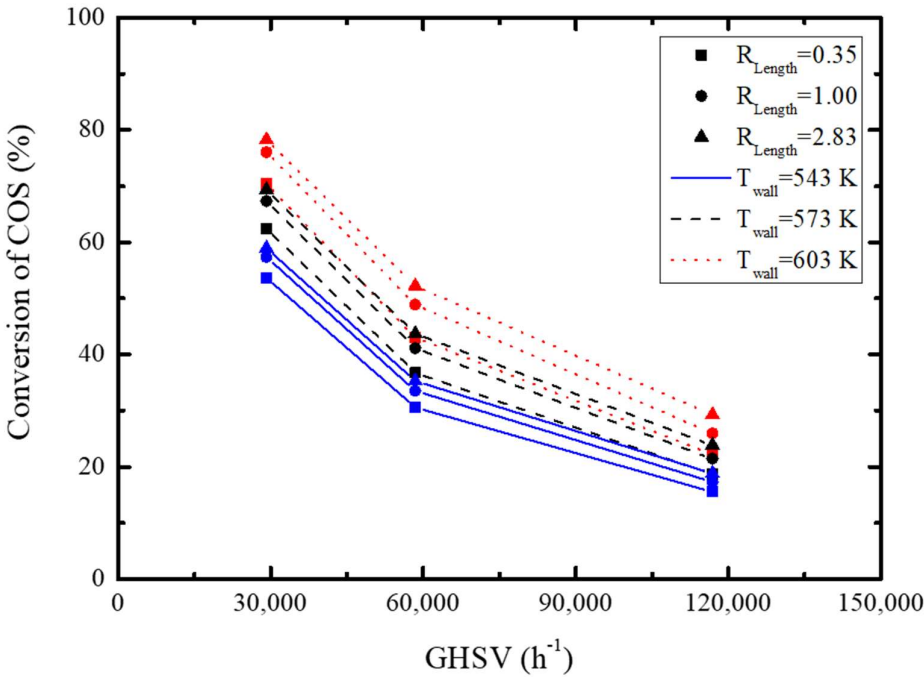


Figure 6

(a)



(b)

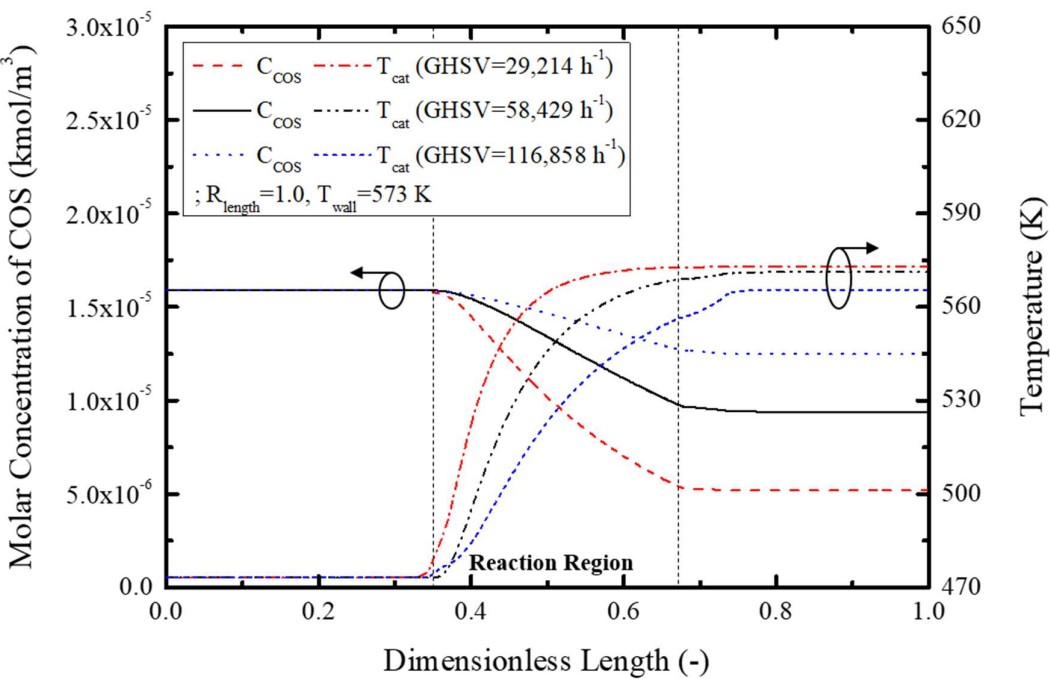
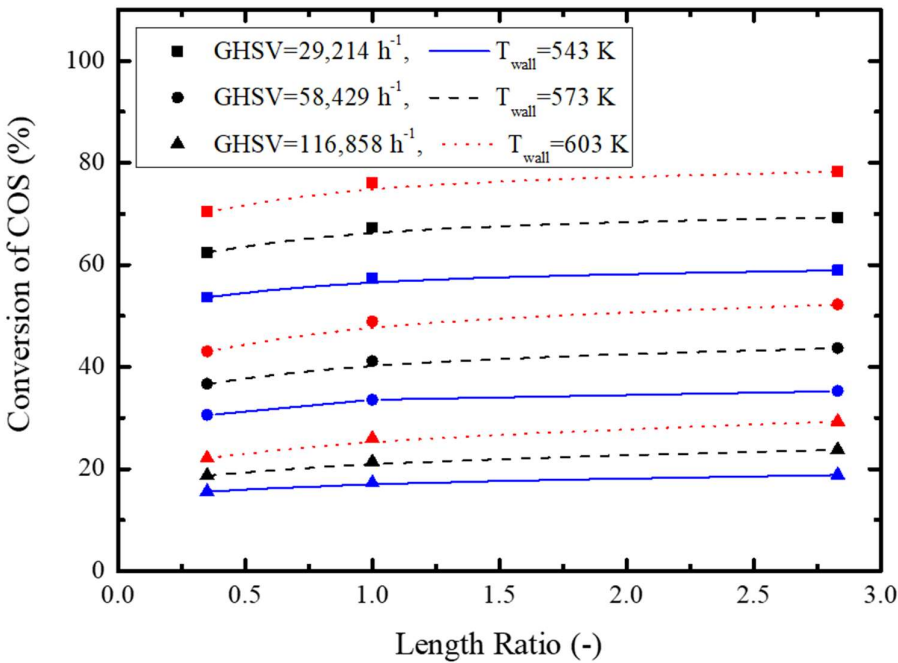


Figure 7

(a)



(b)

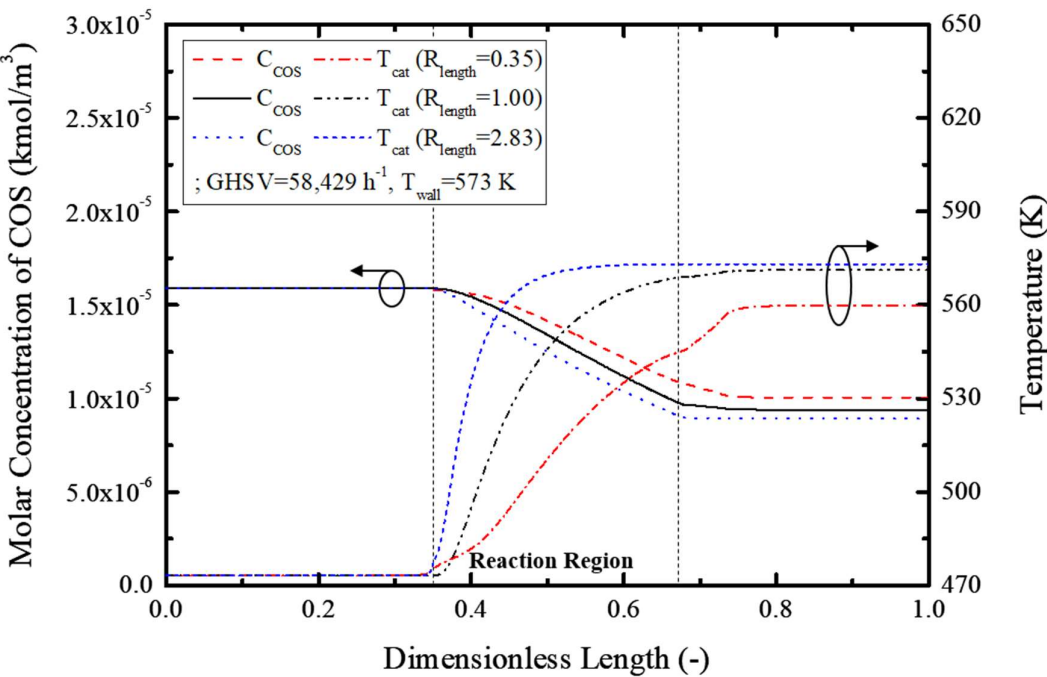
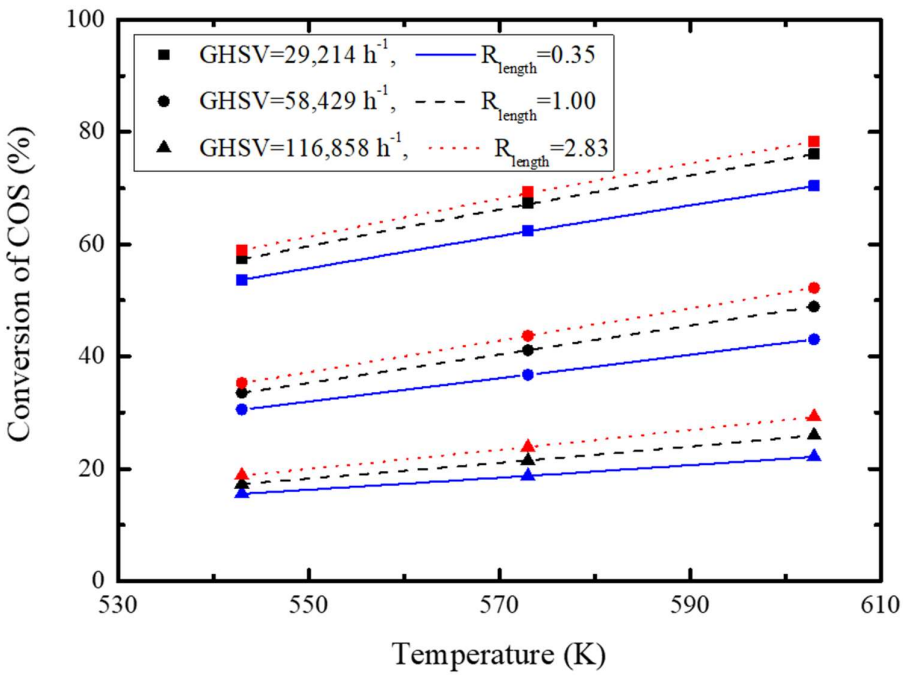


Figure 8

(a)



(b)

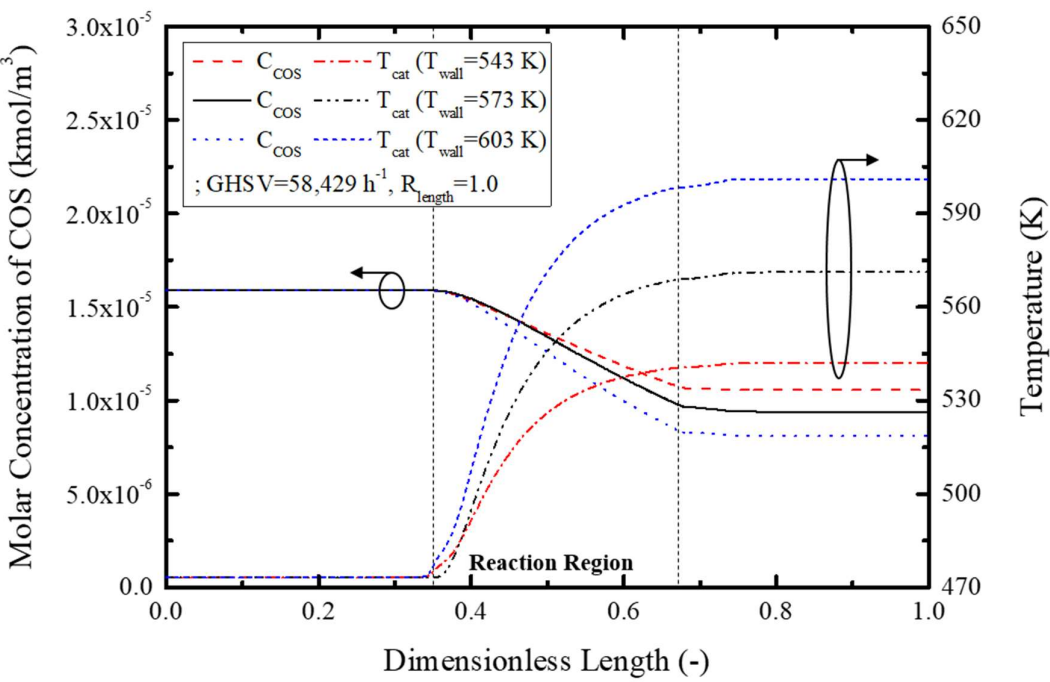


Figure 9

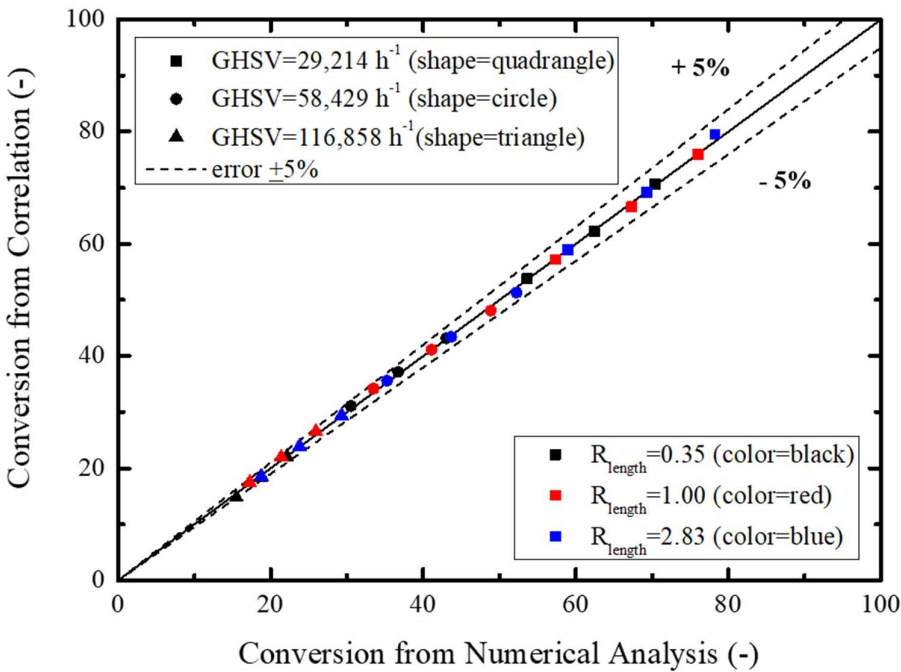
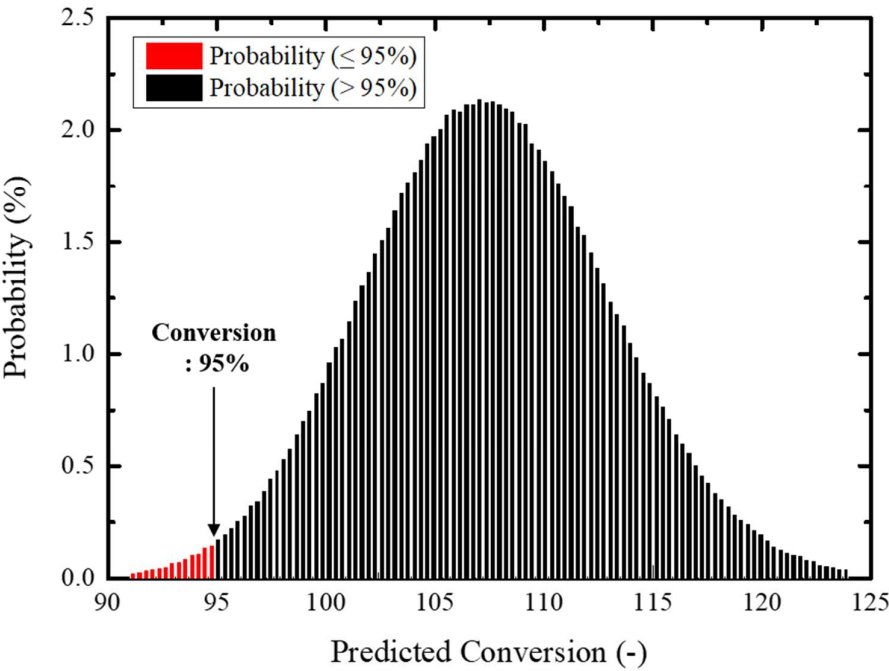


Figure 10

(a)



(b)

